03,09

NV^--centers in diamond and silicon carbide as the basis for room-temperature masers

© Yu.A. Uspenskaya[1], A.S. Gurin[1], M.V. Uchaev[1], A.P. Bundakova[1], M.V. Muzafarova[1], E.N. Mokhov[1], S.S. Nagalyuk[1], V.A. Soltamov[1], P.G. Baranov[1], P.A. Babunts[1], S.Ya. Kilin[2]

[1] Ioffe Institute,
St. Petersburg, Russia
[2] National Research Nuclear University „MEPhI",
Moscow, Russia

E-mail: yulia.uspenskaya@mail.ioffe.ru

Received August 20, 2025
Revised August 20, 2025
Accepted August 23, 2025

The successful realization of coherent microwave amplification (maser effect) at room temperature (300 K) based on optically aligned triplet spin sublevels of negatively charged nitrogen-vacancy centers (NV^-) in diamond marked a new milestone in the development of solid-state masers. In this paper, we present a comparative analysis of the spin-optical properties of NV^- centers in diamond and NV^- centers in silicon carbide (SiC) with a reduced content of the magnetic isotope ^{29}Si ($I = 1/2$), which are used to create masers operating at room temperature. The similarity of the optical pumping mechanisms that form the inverse population of the ground triplet state in both systems is demonstrated. The transverse spin relaxation times $T_2^* \approx 1.5\,\mu s$ for NV^--centers in isotopically modified ^{28}SiC significantly exceed the corresponding values for diamond ($T_2^* \approx 0.3\,\mu s$). The longitudinal relaxation times are comparable with the requirements for maintaining the population inversion: about 1.5 ms for NV^- in diamond and 100 μs for NV^- in ^{28}SiC. The combination of the ability to grow large SiC single crystals and the high permissible concentration of active centers opens up prospects for creating a scalable and technologically efficient platform for solid-state masers operating at room temperature.

Keywords: maser, electron paramagnetic resonance, diamond, silicon carbide, nitrogen-vacancy defect.

DOI: 10.61011/PSS.2025.09.62350.233-25

1. Introduction

Masers, i. e. instruments that are based on coherent amplification of microwaves by stimulated radiation, are important platforms for supersensitive measurements of weak fields, precise spectroscopy and frequency metrology [1–3]. A solid-state maser is classically exemplified by Al_2O_3 ruby crystals with ions of Cr^{3+} that has a quartet spin ground state ($S = 3/2$) [4,5], which are applied in long-range space communication systems, radio astronomy [6–8]. The main condition for origination of maser generation is creation of long-lived population inversion of spin sublevels that are characterized by splitting in the microwave range, which is created under effect of external magnetic and crystal fields. When inversion is available, the weak microwave field that passes through an active medium induces stimulated transitions which are accompanied by emission of photons of the same frequency and phase as the exciting field, thereby resulting in coherent amplification of the microwave signal. When placed within a resonant cavity with a quality factor Q, this amplification is enhanced through multiple passes. If the energy delivered by the spin centers exceeds the internal losses of the cavity, the system reaches the threshold for self-sustained oscillation, entering a stable maser generation mode. Beyond achieving a population inversion, the transition to a maser generation mode requires several physical conditions to be met. These include the frequency matching of the microwave field with the resonant transition, a long spin-lattice relaxation time (T_1), and high phase coherence (T_2^*). Furthermore, internal losses within the resonant cavity must be minimized, as dictated by the quality factor (Q). These interdependent requirements are captured by the dimensionless cooperativity parameter (C), which defines the system's ability to overcome cavity losses and sustain oscillation. The cooperativity parameter is calculated using the following formula

$$C = \frac{4g_s^2 N}{k_s k_c},$$

where $k_s = 2/T_2^*$, $k_c = \omega_c/Q$, g_s is a relation of one spin with the resonant cavity mode, ω_c is a frequency of the resonance mode, N is a number of active centers [9].

Implementation of maser generations requires fulfilment of the condition $C > 1$, at which amplification by the active medium exceeds the losses in the resonant cavity. Even when exceeding a threshold value of amplification $C > 1$ stable stimulated emission is only possible when there is pumping that provides permanent population inversion. A condition of its efficiency is formulated via a minimum required pumping frequency: $\varpi_{thr} = \frac{1}{T_1 K(C-1)}$, where T_1 is a longitudinal time of spin relaxation and K is a pumping efficiency coefficient that characterizes probability

of conversion of the system into an inverse spin state. This expression presents a fundamental requirement: the pumping rate shall exceed a rate of spontaneous relaxation in order to preserve inversion and to provide conditions for the stable generation mode. When considering cooperativity and the threshold pumping frequency ϖ_{thr}, it is obvious that the relaxation times T_1 and T_2^* of the active centers as well as their numbers directly determine implementability of the not laser, but maser effect and its efficiency. The resonant cavity Q factor varies within the range from 10^3 to 10^9 [10] in a dependence from a technical solution and does not directly belong to spin and optical properties of the active medium. It is a combination of intrinsic properties of paramagnetic centers and methods of creation of inverse population that results to the fact that the masers based on transition metal ions in Al_2O_3 operate at the liquid helium temperature. Thus, inverse population of the spin sublevels of Cr^{3+} is achieved during microwave pumping when $T \lesssim 4\,\mathrm{K}$ [5,6,8,11]. According to the Boltzmann statistics, at this temperature the ions predominantly stay at a lower level of a spin quartet. This provides high polarization and effective transfer of pumping to higher levels. The low temperature is critical for creating non-equilibrium distribution that provides operation of the Cr^{3+} masers. Within the specified temperature range, T_1 durations span from several to hundreds of milliseconds [11,12], while T_2^* is approximately 10 ns [8]. The second method of creating inverse population in systems of the $Al_2O_3:Cr^{3+}$ type includes optical pumping of the ground state [13]. However, at the temperatures above 50 K the electron spin system of the chromium ions exhibits large shortening of spin-lattice relaxation according to the dependence $T_1 \propto T^{-7}$, while at the liquid nitrogen temperature the relaxation time T_1 is about $17\,\mu$s [11,12]. A further increase toward room temperature results in a significant shortening of this decay time to $3\,\mu$s [11]. As a result, the maser effect can not obtained at the high temperatures due to short T_1 that limits the lifetime of the inverse state.

It follows from the foregoing that in order to implement the maser operating at the room temperature, the amplifying spin system shall combine: long times T_1 and T_2^*; effective optical pumping resulting in inverse population of the spin sublevels; a sufficient concentration of the active centers. Fulfilment of all these conditions made it possible to realize the first pulse solid-state maser operating at the room temperature, where pentacene molecules ($N = 0.01\,\%$) in a single-crystal organic matrix of para-terphenyl were used as an amplifying medium [14]. Due to optical pumping, it was possible to create inverse population between metastable triplet sublevels of the pentacene molecules with the lifetime $T_1 \approx 45\,\mu$s. Combined with a quite long time of phase coherence $T_2^* \approx 400$ ns [15] and use of the high-Q ($Q = 1.8 \cdot 10^5$) resonant cavity, it made it possible to obtain coherent microwave pulses of duration of about $450\,\mu$s at the frequency of 1.45 GHz at $T \approx 300$ K. Thus, it is evident that optically polarized spin states with the properties listed above can serve as a foundation for designing highly

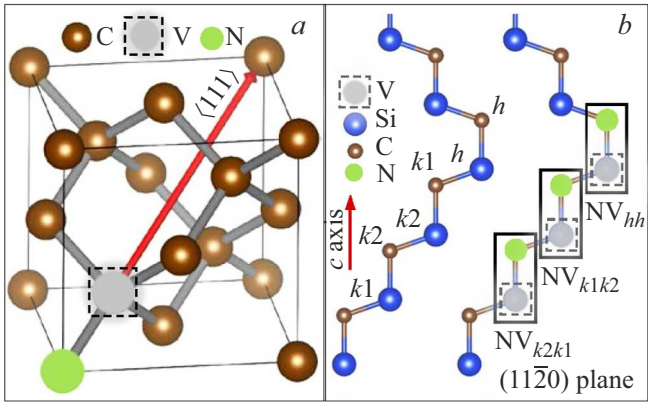

Figure 1. (a) Microscopic model of the NV-center in the diamond lattice. The crystallographic direction $\langle 111 \rangle$ is indicated by a red arrow.(b) Structure of the 6H-SiC lattice in the plane $(11\bar{2}0)$. The direction of the hexagonal axis c is shown by the red arrow. The nonequivalent positions are designated: a hexagonal one (h) and quasi-cubic ones (k_1, k_2).

efficient masers operating at room temperature. For these purposes, it was proposed to use optically-generated triplet ($S = 1$) spin states of the negatively-charged nitrogen-vacancy centers (NV^-) in diamond [16] and quartet states ($S = 3/2$) of silicon vacancies in silicon carbide (SiC) [17]. Both the types of these centers have long times of coherence at the room temperature and optically-induced inverse population of the spin sublevels [16,18]. Thus, the typical times T_1 and T_2^* are about 2–5 ms and 200–500 ns [19–21], respectively, for ensembles of the NV^--centers in diamond. The following relaxation times T_1 and T_2^* are observed for ensembles of the V_{Si}^- centers in SiC: 100–300 μs [22,23] and 250–300 ns [24,25], respectively. It made it possible to demonstrate maser generation using such active media as diamond (NV^-) [20] and silicon carbide (V_{Si}^-) [25]. It is especially important to achieve the maser effect at the room temperature both in organic and inorganic crystals, i. e. without using cryogenic technology [9,26–29].

Silicon carbide is of considerable interest as a technologically mature semiconductor material, supported by established industrial processes for growing bulk single crystals with diameters exceeding 4 inches and highly reproducible parameters Methods of microwave and optical spectroscopy showed that SiC has the NV^--centers that are similar to the NV^--centers in diamond in terms of their nature, structure and spin properties [30–32]. Figure 1 shows microscopic models of these centers in the lattice of diamond and silicon carbide of the polytype 6H. The NV-center in SiC is a complex that consists of a negatively charged silicon vacancy (V_{Si}-) and a nitrogen atom nearest thereto in a position of substitution of the carbon atom (N_C) [30–32]. Since the polytype 6H-SiC is characterized by availability of three non-equivalent crystallographic positions: a hexagonal one (h) and two quasi-cubic ones ($k1$, $k2$), then the NV-centers in 6H can be formed in configurations that

include three axial ones (NV_{hh}, NV_{k2k1}, NV_{k1k2}) and three basal ones (NV_{hk1}, NV_{k1h}, NV_{k2k2}).

Within its framework, the present study will consider only an axial configuration NV_{k1k2}, which is exemplified to comparatively analyze the spin and optical properties of the NV-centers in diamond and in an isotope-modified 6*H*-^{28}SiC with a reduced content of a magnetic isotope ^{29}Si ($I = 1/2$) in order to demonstrate viability of the system 6*H*-^{28}SiC : NV^- as the active medium for the masers operating at the room temperature [33].

2. Experimental

Crystals of silicon carbide 6*H*-^{28}SiC with a reduced content of a silicon magnetic isotope ^{29}Si ($I = 1/2$) were produced by sublimation deposition from a vapor phase at the high temperatures (Physical Vapour Transport — PVT) [34] using a precursor enriched with a nonmagnetic isotope ^{28}Si. A standard plate 6*H*-SiC with the following isotope composition was used as a seed substrate: ^{29}Si (4.7 %, $I = 1/2$), ^{28}Si (92.2 %, $I = 0$), ^{30}Si (3.1 %, $I = 0$) as well as carbon isotopes ^{12}C (98.9 %, $I = 0$) and ^{13}C (1.1 %, $I = 1/2$). A source of the isotope ^{28}Si was a commercially available powder precursor with 99.98 % purity in terms of the content of this isotope. Thus, the concentration of the isotopes ^{29}Si and ^{30}Si in the initial material were reduced by more than an order as compared to their natural content. In order to create the NV^--centers, the grown samples were irradiated with electrons of the energy of 2 MeV at a dose of $2 \cdot 10^{18}$ cm^{-2} and after that they were annealed for two hours at the temperature of 900 °C in the argon atmosphere. Experiments by electron paramagnetic resonance (EPR) were performed in a continuous and a pulsed mode using commercial spectrometers Bruker ESP300 and E680 within the frequency ranges 9.4 GHz (X-range) and 94 GHz (W-range), respectively. The EPR spectra were recorded in the pulsed mode by measuring integral intensity of the signal of electron spin echo (ESE) in a dependence on the magnetic field **B** using the Khan sequence: $\pi/2-\tau-\pi-\tau-$ESE. Duration of the $\pi/2$-pulse was 44 ns, while the delay $\tau = 280$ ns. The sequence is shown schematically in the insert of the Figure 2, *a*. The studies were performed at the room temperature ($T = 300$ K) using optical excitation by lasers of the wavelength of 532 nm for the NV^- centers in diamond and of 980 nm for the NV-centers in SiC.

3. Results and discussion

Figure 2 shows spectra of electron spin echo of the NV^--centers in diamond and SiC, which are recorded within the W range at the temperature of $T = 300$ K with optical excitation by the laser $\lambda = 532$ nm. A set of the axial NV^- centers in SiC is indicated by arrows, splitting between the EPR spectral lines on the magnetic field corresponds to a double value of splitting of the spin sublevels of the triplet ($S = 1$) in the zero magnetic field (Zero Field Splitting — ZFS), which is schematically designated in Figure 2, *c* as *D*. Namely, $\Delta B \cong 2D/g\mu_B$, where *D* is a ZFS value, *g* is an electron g-factor ($g \approx 2.00$), μ_B is a Bohr magneton. The parameters *D*, which are determined by this way, have the following values: for NV_{hh}: $D \approx 1.33$ GHz; for NV_{k2k1}: $D \approx 1.28$ GHz; for NV_{k1k2}: $D \approx 1.36$ GHz. The obtained results fully agree with data previously specified by methods of microwave spectroscopy [31,35,36]. The EPR signals of the NV^--centers are observed both in diamond and in SiC. It makes sense to consider the spectral lines with maximum splitting between the fine structure components in the magnetic field, which corresponds to the NV-centers oriented along the direction ⟨111⟩ of the diamond lattice, which coincides with the direction of the constant magnetic field. The ZFS parameter for the NV^--centers in diamond has a value $D = 2.87$ GHz [16]. Since splitting between the spectral lines in the experiment is 195.9 mT (Figure 2, *b*), it can be found that a deviation of the magnetic field is about 9.5° from the ideal orientation. A key feature of the spectra in both SiC and diamond is the pronounced spin polarization of the ground state. This is achieved via spin-dependent optical pumping through a nonradiative recombination pathway from the excited ^3E state. This process occurs via a metastable state (MS) through intersystem crossing, which selectively repopulates the ground-state spin levels. A cycle of optical pumping is schematically shown in Figure 2, *c* and it results in predominant population of the spin sublevel $m_S = 0$, forming inverse population relative to a state with projection of the spin $m_S = -1$.

Creation of inverse population is well observed in the EPR spectra due to inversion of phases of the magnetic resonance signals of the same-name centers in the low and high magnetic fields. At the same time, resonance radiation of the microwaves is recorded at the high-field components that correspond to the transition $m_S = 0 \leftrightarrow m_S = -1$, which is illustrated by a diagram shown in Figure 2, *c*. Thus, the main requirement for maser creation, which is related to population inversion in the NV-centers in SiC, is realized by the recombination mechanism that it typical for the NV^--centers in diamond, and inversion occurs in relation to the sublevel $m_S = -1$.

Let us consider hyperfine interaction (HFI) of the electron spin of the NV-centers in the crystal matrices with the intrinsic nuclear spin of the nitrogen atom included in the NV-center. Since the isotope ^{14}N has the nuclear spin $I = 1$, then for the considered centers the hyperfine structure (HFS) will consists of the three equidistant lines ($n = 2I + 1$) with splitting between the lines being equal to a value of HFI characterized by the constant *A*. This is clearly see in Figure 2, *d*. One can also note that both HFI and a width of the hyperfine components of the NV^--centers in 6*H*-^{28}SiC is much less than similar parameters for the NV^--centers in diamond. Namely, $A(^{14}\text{N})$ in SiC is just 1.20 MHz, whereas for diamond $A(^{14}\text{N}) \approx 2.24$ MHz, which agrees with results of electron nuclear double resonance experiments [37–39]. Thus, the

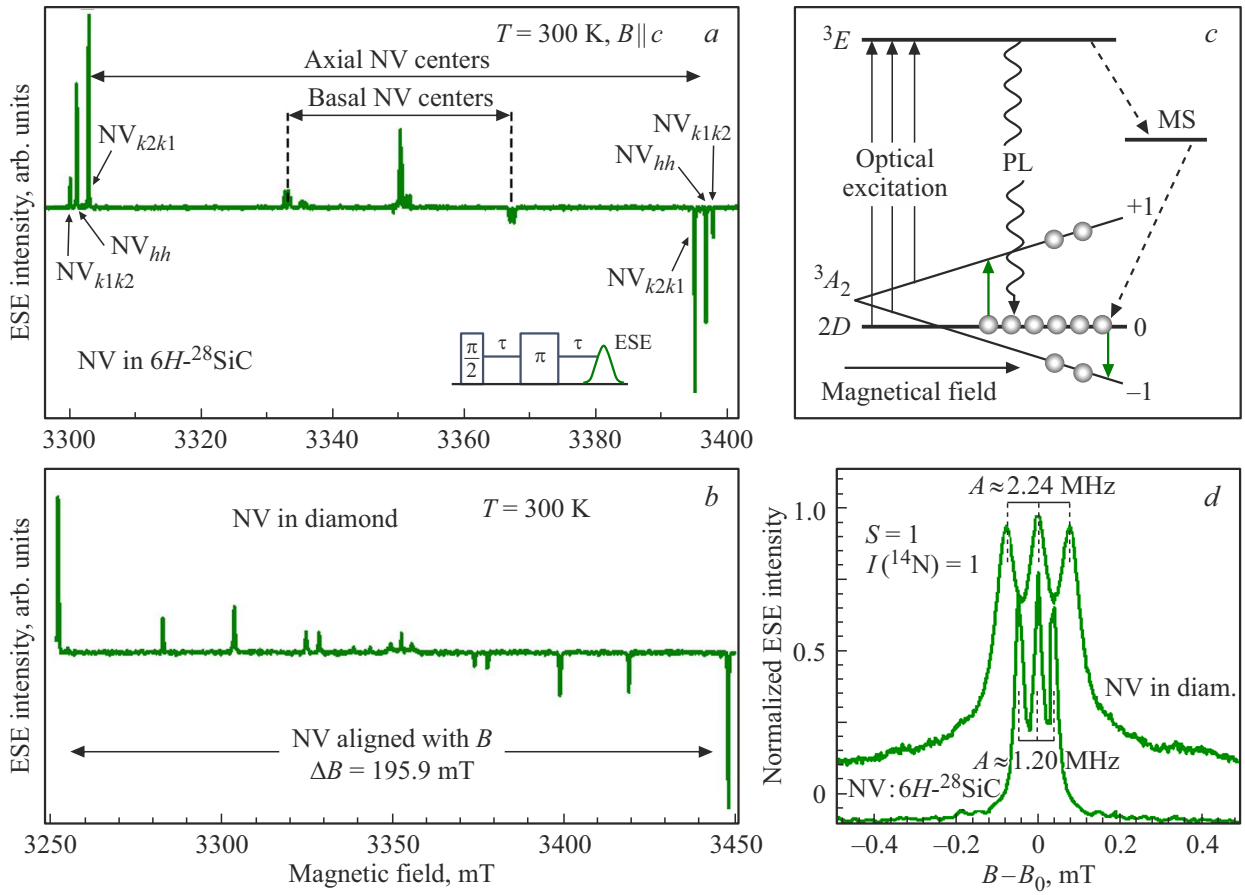

Figure 2. (*a*) EPR spectrum of the NV$^-$-centers in 6*H*-^{28}SiC, which is recorded in orientation of the external magnetic field **B** ∥ **c** and at optical excitation $\lambda = 532$ nm. The insert shows a Khan pulse sequence used for recording the EPR spectra of the NV$^-$-centers in diamond and SiC. The EPR signals of the axial and basal NV$^-$-centers are designated by horizontal arrows. Magnetic dipole transitions between the spin sublevels of the axial centers in the low ($m_S = 0 \leftrightarrow m_S = +1$) and high ($m_S = 0 \leftrightarrow m_S = -1$) magnetic fields are designated by arrows: NV$_{hh}$, NV$_{k2k1}$, NV$_{k1k2}$. (*b*) EPR spectrum of the NV$^-$-centers in diamond, which is recorded with orientation of the field **B** with a deviation of ±9.5° from the axis ⟨111⟩ of the diamond lattice. The horizontal arrow shows transitions between the spin sublevels of the NV$^-$-centers $m_S = 0 \leftrightarrow m_S = +1$ and $m_S = 0 \leftrightarrow m_S = -1$, with the main z-axis of the **D**-tensor, which coincides with the direction of the magnetic field. (*c*) Diagram of a process of optical pumping of the spin sublevels of the NV$^-$-centers in diamond and in SiC. Optical excitation from the ground state (^{3}A$_2$) into the excited one (^{3}E) is shown by a vertical arrow. A channel of nonradiative spin-dependent recombination from ^{3}E into ^{3}A$_2$ via a metastable state (MS) is shown by dashed arrows. Spin-dependent photoluminescence is designated as PL. Predominant population of the sublevel $m_S = 0$ in ^{3}A$_2$ is schematically shown by circles. The green arrows show allowed EPR transitions with taking into account their inverse nature. Splitting of the spin sublevels in a zero magnetic field is designated as D. (*d*) Three HFS lines that occur due to interaction of the electron spin of the NV-centers with a nuclear spin of ^{14}N ($I = 1$). The spectra are constructed in the coordinates $\mathbf{B} - \mathbf{B}_0$, where $\mathbf{B}_0$ corresponds to values of resonance magnetic fields of the central HFS components ($m_S = 0$, $m_I = 0$) ↔ ($m_S = 1$, $m_I = 0$) in diamond and in 6*H*-^{28}SiC. The hyperfine structures are designated by dashed lines with specifying the constant A in MHz.

value of HFI of the NV$^-$-center in diamond with ^{14}N in two times exceeds the similar value for the NV$^-$-center with ^{14}N in SiC. Both HFI with ^{14}N and mechanisms of heterogeneous broadening of the magnetic resonance lines are limiting factors of effective transverse time of spin relaxation (phase coherence), which is defined as $T_2^* = 1/(\gamma_e H_{1/2})$, where $H_{1/2}$ is a width of the line at half maximum in units of the constant magnetic field, while γ_e is a gyromagnetic ratio for an electron. It is obvious that a parameter T_2^* that is crucial for maser implementation in case of the NV$^-$-centers in 6*H*-^{28}SiC is more preferable, which makes this system more promising for practical application.

It is worth emphasizing similarity of these two centers in the crystal matrices of diamond and SiC, which is well traced on the example of analysis of such a parameter as splitting in the zero magnetic field (the parameter D). Taking into account that in the ground state of the centers splitting is predominantly defined by spin-spin interaction [40], it is possible to directly analyze scaling of the value of this interaction when transiting from the diamond lattice to the SiC lattice. Let us start from analyzing the

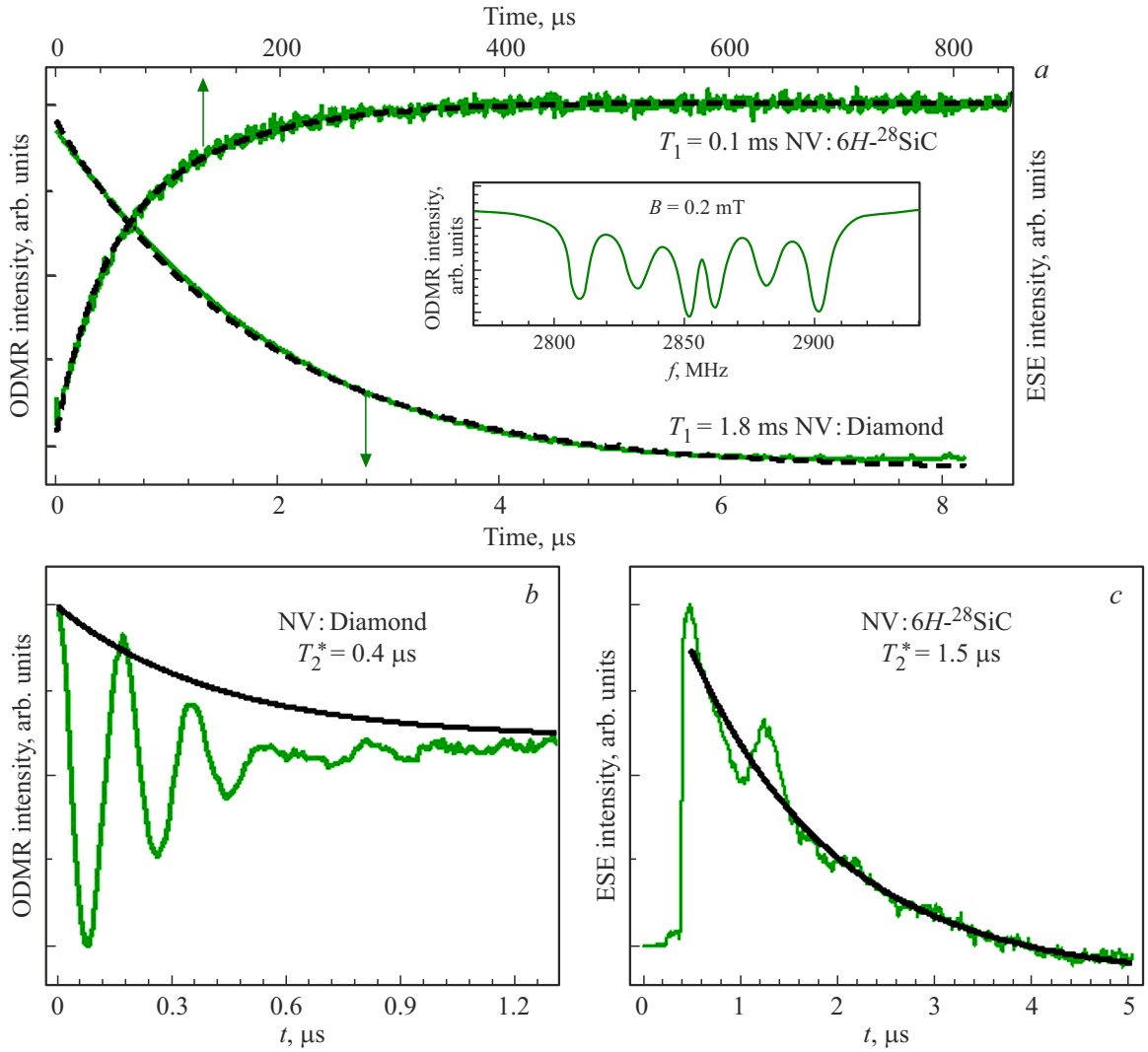

Figure 3. (*a*) Dependences of spin-lattice relaxation, which are measured for the NV^--centers in diamond and for NV_{k2k1} in 6*H*-^{28}SiC by methods of electron spin echo in the W range and ODMR in the magnetic field $\mathbf{B} = 0.2$ mT, respectively. The insert includes an ODMR spectrum and a dashed line shows a signal frequency, at which relaxation characteristics were measured. A pulse sequence was used to record a curve of relaxation of the NV_{k2k1}-centers by variation of an amplitude of spin echo in a dependence on the delay time Δ after an inverting π pulse. $\pi-\Delta-\pi/2-\tau-\pi-\tau-$ESE. Magnetic dipole transition $m_S = 0 \leftrightarrow m_S = -1$ was used for determining the relaxation time of the NV^--centers in diamond by the ODMR method. The following sequence of the microwave pulses was used: $\pi-\Delta-\pi/2-\tau-\pi-\tau-\pi/2-$ODMR, in which the last $\pi/2$ pulse was applied for transferring coherence into population of the state $m_S = 0$. (*b*) Rabi oscillations observed at excitation of the transition $m_S = 0 \leftrightarrow m_S = -1$ by a resonance MW pulse of variable duration $t + \Delta t$ in the magnetic field $\mathbf{B} = 0.2$ mT. (*c*) The free induction decay (FID) signal of the NV_{k2k1}-centers, which is recorded at a low-field component of the fine structure following the microwave excitation pulse.

value of D in diamond: $D = \frac{3\mu_0}{16\pi h} \cdot \frac{(g\mu_B)^2}{\langle r \rangle^3}$, where $\langle r \rangle$ is an average distance between unpaired electrons. Using this approximation and the value $D = 2.87$ GHz for the NV^--center in diamond [16,38], one can determine that the average distance between the unpaired electrons that form the triplet is about 2.4 Å, which is comparable to the distance of 2.43 Å between the basal carbon atoms surrounding the carbon vacancy, on which a major part of the spin density is localized. In 6*H*-SiC, this distance is bigger and is about 3.08 Å. Thus, it can be assumed that for the NV-centers in 6*H*-SiC the ZFS value will be approximately in $(3.08/2.43)^3 \approx 2.18$ times less, i.e. about 1.32 GHz. This value well agrees with the experimental data obtained for the NV-centers in 6*H*-^{28}SiC and clearly demonstrates structure similarity of these centers in diamond and SiC. Consistency is achieved by directly recalculating the main spectroscopic parameter D via the crystal parameters of the matrix.

After analyzing similarity of the optical and spin properties of the NV-centers in SiC and diamond, we present a comparative analysis of their spin dynamics. It is studied by measuring the times of spin-lattice relaxation and phase

memory. The results obtained are shown in Figure 3. Figure 3, $a-c$ shows the experimental data in green and approximation by a monoexponential function in black.

The experimental data for measuring the longitudinal time of relaxation in SiC were approximated by the biexponential function $I(\Delta) = I_0 + A_1 \cdot e^{(-\Delta/T_1)} + A_2 \cdot e^{(-\Delta/T_1')}$ with the characteristic times of spin-lattice relaxation $T_1 = 0.1$ ms and $T_1' = 32\,\mu$s. The time of spin-lattice relaxation $T_1 = 1.86$ ms for the NV-centers in diamond was obtained by approximating the relaxation curve with the monoexponential function $I(\Delta) = I_0 + B \cdot e^{(-\Delta/T_1)}$. The Rabi oscillations and the curve drop of free induction were approximated by the monoexponential function $I(t) = I_0 + C \cdot e^{(-t/T_2^*)}$ to reveal the times of phase memory $T_2^* = 0.4\,\mu$s and $T_2^* = 1.5\,\mu$s for the NV^--centers in diamond and $6H$-^{28}SiC, respectively. Thus, the NV^--centers in $6H$-^{28}SiC are characterized by the shorter times of spin-lattice relaxation T_1 as compared to the similar centers in diamond. However, in spite of this, they have a significantly long time of phase memory that exceeds typical values for the NV^--centers in diamond in 3–5 times. Thus, one may conclude that the NV^--centers in the isotope-purified matrices of silicon carbide are a promising platform for implementing the masers operating at the room temperature. This conclusion is confirmed by experimental results for maser generation on the silicon vacancy centers V_{Si}^- in silicon carbide. Despite exhibiting T_1 relaxation durations analogous to NV^- centers in $6H$-^{28}SiC, these defects possess a significantly shorter phase memory, typically ranging between 250–300 ns.

4. Conclusion

The study has comparatively analyzed the spin and optical properties of the NV^--centers in diamond and the isotope-modified silicon carbide $6H$-^{28}SiC. Special attention was paid to evaluating their viability as the active medium for creating the solid-state masers operating at the room temperature. Despite the shorter spin-lattice relaxation times (T_1) of NV^- centers in $6H$-^{28}SiC compared to similar centers in diamond, their phase coherence time is significantly longer ($1.5\,\mu$s vs. $\sim 0.4\,\mu$s). This is attributed to the weaker hyperfine coupling with the nitrogen nuclear spin within the center's structure, as well as a reduction in inhomogeneous broadening achieved through the use of an isotopically purified matrix. The high structural and spectroscopic identity of these centers, combined with an optical pumping mechanism that creates a population inversion in the triplet ground state similar to that observed in diamond, positions $6H$-^{28}SiC : NV^- as a promising alternative to diamond for next-generation masers. The primary advantages of SiC include its technological scalability and the availability of large-scale single crystals. Taken together, these factors pave the way for the development of compact, stable, and energy-efficient solid-state masers designed for room-temperature operation.

Funding

This study was supported by the Ministry of Science and Higher Education of the Russian Federation (agreement on provision of the grant No. 075-15-2024-556).

Conflict of interest

The authors declare that they have no conflict of interest.

References

[1] N. Basov, A. Prokhorov. J. Exp. Theor. Phys. **1**, 185 (1955).
[2] J.P. Gordon, H.J. Zeiger, C.H. Townes. Phys. Rev., **99**, 1264 (1955).
[3] C. Audoin, J. Vanier. J. Phys. E: Sci. Instrum. **9**, 697 (1976).
[4] G. Makhov, C. Kikuchi, J. Lambe, R.W. Terhune. Phys. Rev. **109**, 1399–1400 (1958).
[5] H.E.D. Scovil, G. Feher , H. Seidel. Phys. Rev. **105**, 762 (1957).
[6] R.C. Clauss, J.S. Shell. Ruby masers. In Low-Noise Systems in the Deep Space Network (ed. Reid, M.S.) (Deep Space Communication and Navigation Series, Jet Propulsion Laboratory, Caltech, 2008).
[7] R. Forward, F. Goodwin, J. Kiefer. „Application of a solid-state ruby maser to an X-band radar system," in WESCON/59 Conference Record (IEEE, 1959), Vol. 3, pp. 119–125.
[8] A. Sigmen. Mazery. — M., Mir, 1966 (in Russian).
[9] D.M. Arroo, N.McN. Alford, J.D. Breeze. Appl. Phys. Lett. **119**, 140502 (2021);
[10] A. Barannik, N. Cherpak, A. Kirichenko, Y. Prokopenko, S. Vitusevich, and V. Yakovenko. Int. J. Microwave Wireless Technol. **9**, 781–796 (2017).
[11] G.M. Zverev, Sh.V. Marlov, L.S. Kornienko, A.A. Maienkov, A.Sh. Prokhorov. UFN, **77** 61–108 (1962). (in Russian).
[12] J.H. Pace, D.F. Sampson, J.S. Thorp. Phys. Rev. Lett. **4**, 18 (1960).
[13] H. Hsu, F.K. Tittel. Optical pumping of microwave masers. Proc. IEEE **51**, 185–189 (1963).
[14] M. Oxborrow, J.D. Breeze, N.M. Alford. Nature **488**, 353–356 (2012).
[15] A. Mena, S.K. Mann, A. Cowley-Semple, E. Bryan, S. Heutz, D.R. McCamey, M. Attwood, S.L. Bayliss. Phys. Rev. Lett. **133**, 120801 (2024)
[16] J. Loubser, J. Van Wyk. „Optical spin-polarisation in a triplet state in irradiated and annealed type 1b diamonds", Diamond Res. 1977, 11–14.
[17] H. Kraus, V. Soltamov, D. Riedel, S. V€ath, F. Fuchs, A. Sperlich, P. Baranov, V. Dyakonov, G. Astakhov. Nat. Phys. **10**, 157–162 (2014).
[18] V.A. Soltamov, A.A. Soltamova, P.G. Baranov, I.I. Proskuryakov. Phys. Rev. Lett. **108**, 226402 (2012)
[19] A. Jarmola, V.M. Acosta, K. Jensen, S. Chemerisov, D. Budker. Phys. Rev. Lett. **108**, 197601 (2012)
[20] J.D. Breeze, E. Salvadori, J. Sathian, N. McN. Alford1, C.W.M. Kay. Nature **555**, 493–496 (2018)
[21] V.M. Acosta, E. Bauch, M.P. Ledbetter, C. Santori, K.-M.C. Fu, P.E. Barclay, R.G. Beausoleil, H. Linget, J.F. Roch, F. Treussart, S. Chemerisov, W. Gawlik, D. Budker. Phys. Rev. B **80**, 115202 (2009)

[22] C. Kasper, D. Klenkert, Z. Shang, D. Simin, A. Gottscholl, A. Sperlich, H. Kraus, C. Schneider, S. Zhou, M. Trupke, W. Kada, T. Ohshima, V. Dyakonov,1 V. Astakhov. Phys. Rev. Applied **13**, 044054 (2020)
[23] V.A. Soltamov, B.V. Yavkin, A.N. Anisimov, H. Singh, A.P. Bundakova, G.V. Mamin, S.B. Orlinskii, E.N. Mokhov, D. Suter, P.G. Baranov. Phys. Rev. B **103**, 195201 (2021)
[24] D. Simin, H. Kraus, A. Sperlich, T. Ohshima, G.V. Astakhov, V. Dyakonov. Phys. Rev. B **95**, 161201(R) (2017).
[25] A. Gottscholl, M. Wagenhöfer, V. Baianov, V. Dyakonov, A. Sperlich. arXiv:2312.08251 (2023)
[26] C.B. Rodriguez. arXiv:2308.00848 (2023)
[27] H. Wu, X. Xie, W. Ng, S. Mehanna, Y. Li, M. Attwood, M. Oxborrow. Phys. Rev. Appl. **14**, *6*, 064017 (2020)
[28] H. Wu, S. Mirkhanov, W. Ng, M. Oxborrow. Phys. Rev. Lett. **127**, *5*, 053604 (2020)
[29] Wern Ng, Yongqiang Wen, M. Attwood; D.C. Jones; M. Oxborrow, N. McN. Alford, D. M. Arroo. Appl. Phys. Lett. **124**, 044004 (2024)
[30] H.J. von Bardeleben, J.L. Cantin, E. Rauls, U. Gerstmann. Phys. Rev. B **92**, 064104 (2015).
[31] Kh. Khazen, H.J. von Bardeleben, S.A. Zargaleh, J.L. Cantin,1 Mu Zhao, W. Gao, T. Biktagirov, U. Gerstmann. Phys. Rev. B 100, 205202 (2019).
[32] F.F. Murzakhanov, M.A. Sadovnikova, G.V. Mamin, S.S. Nagalyuk, H.J. von Bardeleben, W.G. Schmidt, T. Biktagirov, U. Gerstmann, V.A. Soltamov. J. Appl. Phys. 134, 123906 (2023).
[33] Patent RF 2523744. Aktivnyi material dlya mazera s opticheskoi nakachkoi i mazer s opticheskoi nakachkoi / P.G. Baranov, R.A. Babunts, A.A. Soltamova, V.A. Soltamov, A.P. Bundakova. Zayavl. 24.08.2012. Opubl. 20.07.2014 (in Russian).
[34] Yu.A. Vodakov, E.N. Mokhov, M.G. Ramm, A.D. Roenkov. Krist. Tech., **14**, 729 (1979).
[35] E.N. Mokhov, S.S. Nagalyuk, O.P. Kazarova, S.I. Dorozhkin, V.A. Soltamov. Phys. Sol. St. **67**, *1*, 114–120 (2025).
[36] F.F. Murzakhanov, D.V. Shurtakova, E.I. Oleynikova, G.V. Mamin, M.A. Sadovnikova, O.P. Kazarova, E.N. Mokhov, M.R. Gafurov, V.A. Soltamov. Appl. Magn. Reson. **55**, 1175–1182 (2024).
[37] B.V. Yavkin, G.V. Mamin, S.B. Orlinskii. J. Magn. Reson. **262**, 15 (2016).
[38] X.F. He, N.B. Manson, P.T.H. Fisk. Phys. Rev. B 47, 8809 (1993).
[39] L.R. Latypova, I.N. Gracheva, D.V. Shurtakova, F.F. Murzakhanov, M.A. Sadovnikova, G.V. Mamin, M.R. Gafurov. J. Phys. Chem. C 2024, **128**, *43*, 18559–1856.
[40] T. Biktagirov, W.G. Schmidt, U. Gerstmann. Phys. Rev. Research **2**, 022024(R) (2020).

Translated by M.Shevelev